Chin. J. Astron. Astrophys. Vol. 6 (2006), No. 2, 155–164
(*http://www.chjaa.org*)

Chinese Journal of
Astronomy and
Astrophysics

The Feasibility of Constraining Dark Energy Using LAMOST Redshift Survey *

Lei Sun, Meng Su and Zu-Hui Fan

Department of Astronomy, Peking University, Beijing 100871; *sunl@bac.pku.edu.cn*

Received 2005 August 2; accepted 2005 August 23

Abstract We consider using future redshift surveys with the Large Sky Area Multi-Object Fiber Spectroscopic Telescope (LAMOST) to constrain the equation of state of dark energy ω. We analyze the Alcock & Paczyński (AP) effect imprinted on the two-point correlation function of galaxies in redshift space. The Fisher matrix analysis is applied to estimate the expected error bounds of ω_0 and ω_a from galaxy redshift surveys, ω_0 and ω_a being the two parameters in the equation of state parametrization $\omega(z) = \omega_0 + \omega_a z/(1+z)$. Strong degeneracies between ω_0 and ω_a are found. The direction of the degeneracy in $\omega_0 - \omega_a$ plane, however, rotates counter-clockwise as the redshift increases. LAMOST can potentially contribute in the redshift range up to 0.5. In combination with other high redshift surveys, such as the proposed Kilo-Aperture Optical Spectrograph project (KAOS), the joint constraint derived from galaxy surveys at different redshift ranges is likely to efficiently break the degeneracy of ω_0 and ω_a. We do not anticipate that the nature of dark energy can be well constrained with LAMOST alone, but it may help to reduce the error bounds expected from other observations, such as the Supernova/Acceleration Probe (SNAP).

Key words: Cosmology: theory — galaxies: distances and redshifts — galaxy clustering — large-scale structure of Universe

1 INTRODUCTION

Under the current theoretical framework, the accelerating expansion of the universe directly probed by Type Ia supernovae observations necessitates the existence of dark energy with negative pressure (Riess et al. 1998; Garnavich et al. 1998; Perlmutter et al. 1999; Knop 2003; Riess et al. 2004). Along with other observations, a concordance cosmological model is revealed, in which the universe is made of $\sim 70\%$ dark energy and $\sim 30\%$ dark matter (e.g., Spergel et al. 2003; Bahcall et al. 1999; Allen et al. 2003; Freedman et al. 2001; Fosalba & Gaztanaga 2004; Padmanabhan et al. 2004).

Understanding the nature of dark energy has become one of the most challenging tasks in both cosmology and theoretical physics. The simplest model of the dark energy is the cosmological constant, which is characterized by the equation of state $p = -\rho$ or $\omega = -1$ in $p = \omega\rho$. Its energy density keeps constant as the universe evolves. While being consistent with current observations (e.g., Seljak et al. 2005), it is facing severe theoretical difficulties, such as the fine tuning problem, and the coincidence problem. To overcome these difficulties, people have proposed various dynamical fields for the dark energy. Quintessence is a time-varying field with $\omega > -1$ (e.g., Ratra & Peebles 1988; Caldwell, Dave & Steinhardt 1998). Phantom models are constructed to have $\omega < -1$ (e.g., Caldwell 2002). The weak tendency shown in the observational analyses that ω changes from

* Supported by the National Natural Science Foundation of China.

$\omega > -1$ to $\omega < -1$ at present triggers theoretical studies to build models with ω crossing -1 (Li, Feng & Zhang 2005; Huterer & Cooray 2005; Caldwell & Doran 2005; Hu 2005).

The existence of dark energy affects the expansion history of the universe, which in turn leaves imprints on the formation of large-scale structures. Therefore to probe the dark energy cosmologically, two different types of observables are desirable. One is related to the global geometry and expansion of the universe. The other is associated with the dynamical evolution of large-scale structures. The luminosity distance measured from Type Ia supernovae (e.g., Riess et al. 2004) and the angular diameter distance from X-ray (Allen et al. 2004) or the joint X-ray and the Sunyaev-Zeldovich effect analysis on clusters of galaxies (Reese et al. 2004) are typical ones of the first type. Seeking for information on dark energy from the redshift evolution of cluster abundance (e.g., Haiman et al. 2001; Fan & Wu 2003), gravitational lensing effects (Jarvis et al. 2005), etc., relates to the second type. However, note that usually both the global properties of the universe and the dynamical evolution of structures take part in the second type of analysis. For cosmological observables, degeneracies often exist between parameters related to the equation of state of dark energy and other cosmological parameters. Therefore, it is necessary to combine different observations together to break the degeneracies as much as possible (e.g., Seljak et al. 2005; Rapetti et al. 2005).

The spatial distribution of galaxies contains abundant cosmological information. The power spectrum that reflects the spatial clustering at different scales is the most studied quantity from galaxy redshift surveys (e.g., Tegmark et al. 2004; Eisenstein et al. 2005). The measured shape of the power spectrum puts a tight constraint on the shape parameter Γ, which depends on $\Omega_m h$ with only the dark matter considered. Here Ω_m is the average matter density of the universe at present in units of the critical density, and h is the present Hubble constant in units of $100\,\mathrm{km\ s^{-1}\ Mpc^{-1}}$. Including the baryonic component, the shape parameter is modified. More importantly, the acoustic oscillations shown in the cosmic microwave background (CMB) analysis leave signatures on the power spectrum of density perturbations (Eisenstein et al. 2005). While it is extremely important cosmologically, the power spectrum is not the only information we can retrieve from galaxy surveys. The isotropic two-point correlation function of galaxies in real space appears distorted in the redshift space due to peculiar motions of galaxies and the Alcock & Paczyński (AP) effect. The distortion itself is valuable in understanding the dynamical evolution of large-scale structures, as well as in constraining cosmological parameters.

Matsubara & Szalay (2003) proposed that an analysis of the AP effect on the luminous red galaxies (LRG) in the Sloan Digital Sky Survey (SDSS) can be a useful probe of dark energy. Our project, the Large Sky Area Multi-Object Fiber Spectroscopic Telescope (LAMOST) resembles SDSS in many aspects. Although there are still uncertainties in the final capabilities of LAMOST, it is worthwhile to investigate its possible potentials in cosmological studies. According to Feng, Chu and Yang (2000), LAMOST aims at deeper redshifts than those of SDSS with the average redshift of its main sample around $z \sim 0.2$, and there still will be a significant number of galaxies even at $z = 0.5$, in the LAMOST sample. The total number of galaxies in LAMOST redshift survey will be about 10^7, which is an order of magnitude higher than that of SDSS. These lead us to expect that LAMOST may do better than SDSS in constraining dark energy parameters with the AP analysis. In this paper, we will investigate the feasibility of using LAMOST redshift survey to probe the nature of dark energy.

This paper is organized as follows. In Section 2, we present the relevant theoretical formulations. Numerical analyses on the possible error bounds of dark energy parameters from LAMOST survey are presented in Section 3. Section 4 summarizes our conclusions.

2 THEORY

Spatial clustering of galaxies can be described by the n-point correlation functions, with $n = 2, 3, ...$ For a Gaussian random field, its statistics is fully characterized by the two-point correlation function. In the current model of structure formation, large-scale structures grew from tiny Gaussian density fluctuations generated during the inflationary stage. Thus on large scales where density perturbations are still linear, Gaussianity is well kept. On small scales, however, nonlinear gravitational instability introduces strong non-Gaussian properties into the spatial distribution of galaxies. Large-scale structures of the universe are statistically isotropic in real space. Then for the two-point correlation function, it should only depend on the absolute separation between the galaxy pair. Specifically, for two galaxies at $\boldsymbol{r}_1$ and $\boldsymbol{r}_2$, respectively, their correlation is a function of $r = |\boldsymbol{r}_1 - \boldsymbol{r}_2|$, and independent of the direction of $\boldsymbol{r}_1 - \boldsymbol{r}_2$.

On the other hand, galaxy redshift surveys directly provide us the distribution of galaxies in redshift space. Different from the one in real space, the correlation function in redshift space is significantly distorted by two effects, namely, the peculiar velocity and the AP effect. As a result, the two-point correlation function in redshift space is generally expressed as $\xi(z_1, z_2, \theta)$, with z_1, z_2 as the redshifts of the two galaxies and θ as the angle between them on the sky. This paper focuses on the AP effect, which will be presented in the following.

2.1 AP Effect

Consider an intrinsically spherical object with its center located at redshift z. If both the redshift difference of its diameter along the line of sight δz and the angle $\delta\theta$ extended perpendicular to the line of sight are much less than unity, the corresponding comoving distances through the center, $x_\parallel$ and $x_\perp$, are given by

$$x_\parallel = \frac{dx(z)}{dz}\delta z = \frac{\delta z}{H(z)}, \qquad x_\perp = d_A(z)\delta\theta, \tag{1}$$

where $x(z)$, $H(z)$ and $d_A(z)$ are the radial comoving distance, the redshift dependent Hubble parameter and the comoving angular diameter distance, respectively. Thus we have

$$\frac{\delta z}{z\delta\theta} = \frac{H(z)d_A(z)}{z}\frac{x_\parallel}{x_\perp}. \tag{2}$$

Since $x_\parallel/x_\perp = 1$ for a sphere, the ratio in redshift space depends only on the combined factor $H(z)d_A(z)$, which is a function of the basic cosmological parameters, such as the matter density Ω_m, the dark energy density Ω_Λ and the equation of state of dark energy ω. The deviation of $H(z)d_A(z)/z$ from unity is often referred to as the cosmological redshift distortion effect, and $H(z)d_A(z)$ is named as the AP factor after Alcock & Paczyński (1979) (see also e.g., Matsubara & Suto 1996).

Originally, Alcock & Paczyński (1979) proposed to apply this method to intrinsically spherical structures formed via gravitational clustering, e.g., superclusters. However, even in a statistical sense, it is not likely that the intrinsic shape of the objects resulting from gravitational collapse is ideally spherical. Then, Matsubara & Suto (1996) proposed to make use of the spatial clustering of quasars and galaxies, which is characterized by correlation functions and can be safely assumed to be statistically isotropic in real space. This is usually called the extended AP effect.

As a cosmological probe, the AP effect has an excellent advantage in constraining the properties of dark energy. It has a dependence on $H(z)$ that is direct and not through an integral of $H(z)$ as in the case of distance measurements. Because $H(z)$ has an integral relation with the equation of state of dark energy $\omega(z)$, distance measurements involve a double-integral smoothing in probing $\omega(z)$, and thus the degree of sensitivity to $\omega(z)$ is inevitably lowered in comparison with the AP effect.

2.2 The Two-Point Correlation Function in Redshift Space

In the framework of the Friedmann-Lemaître universe with dark energy extension, the two-point correlation function in redshift space is given by

$$\begin{aligned}\xi(z_1, z_2, \theta) = D(z_1)D(z_2)\big[&b(z_1)b(z_2)\xi^{(0)}(z_1, z_2, \theta)\\ &+ f(z_1)b(z_2)\xi^{(1)}(z_1, z_2, \theta) + f(z_2)b(z_1)\xi^{(1)}(z_2, z_1, \theta)\\ &+ f(z_1)f(z_2)\xi^{(2)}(z_1, z_2, \theta)\big],\end{aligned} \tag{3}$$

where $b(z)$ is the redshift-dependent linear bias factor, $D(z)$ and $f(z)$ are the linear growth factor normalized to $D(z = 0) = 1$ and its logarithmic derivative, respectively (Matsubara 2004). With the same simplification as that in Matsubara (2004), the functions $\xi^{(n)}$ here take the form of

$$\xi^{(0)}(z_1,z_2,\theta)=\xi_0^{(0)}(x_{12}), \tag{4}$$

$$\xi^{(1)}(z_1,z_2,\theta)=\frac{1}{3}\xi_0^{(0)}(x_{12})+\big(\cos^2\gamma_{12}-\frac{1}{3}\big)\xi_2^{(1)}(x_{12}), \tag{5}$$

$$\begin{aligned}\xi^{(2)}(z_1,z_2,\theta)=&\frac{1}{15}\big(1+2\cos^2\theta\big)\xi_0^{(0)}(x_{12})-\frac{1}{7}\Big[\frac{2}{3}+\frac{4}{3}\cos^2\theta-(\cos^2\gamma_{12}+\cos^2\gamma_{21})\\&+4\cos\gamma_{12}\cos\gamma_{21}\cos\theta\Big]\xi_2^{(1)}(x_{12})+\frac{1}{7}\Big[\frac{1}{5}+\frac{2}{5}\cos^2\theta-(\cos^2\gamma_{12}+\cos^2\gamma_{21})\\&+4\cos\gamma_{12}\cos\gamma_{21}\cos\theta+7\cos^2\gamma_{12}\cos^2\gamma_{21}\Big]\xi_4^{(2)}(x_{12}).\end{aligned} \tag{6}$$

Here the functions $\xi_l^{(n)}$ are defined as

$$\xi_l^{(n)}(x)=\frac{(-1)^{n+l}}{x^{2n-l}}\int\frac{k^2dk}{2\pi^2}\frac{j_l(kx)}{k^{2n-l}}P(k), \tag{7}$$

where j_l is the spherical Bessel function. The variable x_{12} represents the comoving separation of the two points. Based on the current cosmological observation, one can safely assume the involved scales of the correlation function are much smaller than the curvature scale of the universe, i.e., $x_{12}\ll|K|^{-1/2}$. Adopting this approximation, x_{12} is given by

$$\begin{aligned}x_{12}\simeq& d_A(x_{12})\\=&\big[d^2(z_1)+d^2(z_2)-2C(z_1)C(z_2)d(z_1)d(z_2)\cos\theta-Kd^2(z_1)d^2(z_2)(1+\cos^2\theta)\big]^{1/2},\end{aligned} \tag{8}$$

where $d(z)\equiv d_A[x(z)]$ and

$$C(z)\equiv\frac{dd_A}{dx}(z)=\begin{cases}\cos\big[\sqrt{K}x(z)\big] & (K>0),\\ 1 & (K=0),\\ \cosh\big[\sqrt{-K}x(z)\big] & (K<0).\end{cases} \tag{9}$$

The quantity γ_{12} is the angle between the separation x_{12} and the line-of-sight direction to the point of z_1, and is given by

$$\cos\gamma_{12}=\frac{d(z_1)C(z_2)-C(z_1)d(z_2)\cos\theta}{d_A(x_{12})}. \tag{10}$$

The definition of γ_{21} results if interchange z_1 and z_2 in the above.

As pointed out by Mutsubara (2004), the extended AP effect is included in the nonlinear and anisotropic mapping from real space to redshift space by $x_{12}(z_1,z_2,\theta)$ of Equation (8).

In the limit of $x_{12}\ll x_1$ and $x_{12}\ll x_2$, the distant-observer approximation is applicable, under which, $\gamma_{ij}=\pi-\gamma_{ji}$ and $\cos\theta=1$. As a result, the correlation function is greatly simplified, with (Matsubara, Szalay & Pope 2004)

$$\xi(z_1,z_2,\theta)=b_1b_2D_1D_2\sum_{n=0}^{2}c_l^{(n)}\xi_l^{(n)}(x_{12}), \tag{11}$$

$$c_0^{(0)}=\big[1+\frac{1}{3}(\beta_1+\beta_2)+\frac{1}{5}\beta_1\beta_2\big]P_0(\cos\gamma), \tag{12}$$

$$c_2^{(1)}=\big[\frac{2}{3}(\beta_1+\beta_2)+\frac{4}{7}\beta_1\beta_2\big]P_2(\cos\gamma), \tag{13}$$

$$c_4^{(2)}=\frac{8}{35}\beta_1\beta_2P_4(\cos\gamma), \tag{14}$$

where $l=2n$, P_l are Legendre polynomials, and $\gamma\equiv\gamma_{12}$ is the angle between the line of sight and the separation. We abbreviate $b_1=b(z_1), D_1=D(z_1), x_1=x(z_1)$, etc. The functions $\xi_l^{(n)}$ are given by Equation (7).

2.3 Evaluation of the Fisher Information Matrix

To estimate to what extent that LAMOST redshift survey can constrain the cosmological parameters, we assume idealized survey conditions which are expected to be accessible for future LAMOST surveys, and give estimates of the error bounds on the dark energy parameters with a calculation of the Fisher information matrix.

Matsubara & Szalay (2002) proposed a simple method of evaluating the Fisher matrix for a given sample. In this method, the data vector is taken to be pixelized galaxy counts N_i in a survey sample. The correlation matrix is simply given by the correlation function convolved by pixels

$$\begin{aligned} C_{ij} &= \left\langle (N_i - \bar{N}_i)(N_j - \bar{N}_j) \right\rangle \\ &= \frac{\bar{N}_i \bar{N}_j}{v_i v_j} \int_{v_i} d^3 z_1 \int_{v_j} d^3 z_2 \xi(z_1, z_2, \theta_{12}) + \bar{N}_i \delta_{ij}, \end{aligned} \tag{15}$$

where v_i is the volume of the pixel i and $\bar{N}_i$ is the expected number of galaxies in that pixel. The second term is the contribution from shot noise (Peebles 1980). Matsubara, Szalay & Pope (2004) showed that there is no need to perform the direct six-dimensional integration when one can set the spherical smoothing cells in comoving space. In that case, performing the smoothing integrations of Equation (15) is equivalent to just replacing the power spectrum $P(k)$ by $P(k)W^2(k)$ in Equation (7), where $W(x) = 3(\sin x - x \cos x)/x^3$ is the top-hat smoothing kernel in Fourier space and R is the smoothing radius in comoving space. Thus, with a given set of cosmological parameters, one can directly obtain the correlation matrix in the same way as computing the correlation function itself in redshift space.

In the linear regime, the distribution of the number counts n_i is multi-variate Gaussian, in which case the Fisher matrix has a simple form (e.g., Vogeley & Szalay 1996; Tegmark et al. 1997)

$$F_{\alpha\beta} = \frac{1}{2} Tr\Big(\boldsymbol{C}^{-1} \frac{\partial \boldsymbol{C}}{\partial \theta_\alpha} \boldsymbol{C}^{-1} \frac{\partial \boldsymbol{C}}{\partial \theta_\beta} \Big), \tag{16}$$

where C is the theoretical model of the correlation function, and (θ_α) is the given set of model parameters.

Throughout the analysis, we adopt the equation of state of dark energy parametrization (Linder 2003a) $\omega(z) = \omega_0 + \omega_a z/(1+z)$. Consequently there are nine parameters in all in our model: Ω_m, Ω_Λ, ω_0, ω_a, b, $f_B = \Omega_B/\Omega_m$, h, σ_8 and n_s.

3 RESULTS AND DISCUSSION

At present, LAMOST is being built and specific spectroscopic targets have not been finally determined. We assume a similar target selection method for LAMOST survey as the SDSS survey adopts. According to York et al. (2000), the redshift space observations of SDSS survey consist of three samples of objects. The first one is a flux-limited sample containing approximately 10^6 'main galaxies' whose redshift extends up to $z \sim 0.2$. The second sample is the set of approximately 120 000 luminous red galaxies (LRGs), which are selected based on color and magnitude (Eisenstein et al. 2001) with a redshift extending to $z \sim 0.5$. Because of the clever selection criteria, the LRGs set approaches a volume-limited sample up to $z \sim 0.4$ and then becomes flux limited at higher redshifts, because of the signal-to-noise ratio limits of the spectroscopic data. The third sample is the set of approximately 10^5 quasars. In terms of dark energy research, the LRG sample attracts most attention due to a right balance between its number density and redshift depth.

From the results of a mock survey conducted by Feng, Chu & Yang (2000), the mean redshift of LAMOST survey is around $z \sim 0.2$, whereas for the SDSS survey the mean redshift is $z \sim 0.1$. Also, a larger survey area is expected for LAMOST in comparison with that of SDSS (Feng, Chu & Yang 2000), although there are still some uncertainties as we mentioned in Section 1, LAMOST survey has a targeting magnitude limit $B_j \sim 20.5$, while the SDSS limiting magnitude is about 18.9. As a result, LAMOST can potentially do a better job on the observation of LRG sample in the sense that the volume-limited sample can extend to the a redshift higher than that of SDSS. We will study the expected constraints on dark energy parameters with the main sample and the LRG sample expected in LAMOST survey. Even if LAMOST survey cannot select LRGs due to its limited capabilities, our study in this paper can serve as a theoretical guide for designing future redshift surveys.

In the specific calculation of Fisher Matrix, we consider both cases with and without the distant-observer approximation. In the distant-observer approximation, the evaluation of the correlation matrix is drastically simplified as we mentioned above. Since the number of elements of a correlation matrix is the square of the number of cells, $N_{\rm cell}^2$, where $N_{\rm cell} \sim 10^3 - 10^4$ or more, the simplification seems to be especially meaningful when doing the numerical computation. In the case without the approximation, more accurate estimation of the expected error bounds can be obtained, at however, correspondingly larger cost of the CPU time.

3.1 The Case with the Distant-Observer Approximation

Given the LAMOST survey geometry, we divide the whole survey area into five redshift ranges with a redshift interval $\Delta z = 0.1$. The central redshift values of the five ranges are set to be $z_m = 0.1, 0.2, 0.3, 0.4$ and 0.5, respectively. Thus the two nearer ranges are related to the 'main galaxies', the number density of which is conservatively set to be $10^{-3}/(h^{-1}\ \mathrm{Mpc})^3$ in our analysis and the three farther ranges correspond to the LRG sample with a number density of $10^{-4}/(h^{-1}\ \mathrm{Mpc})^3$.

In the distant-observer approximation, Euclidean coordinates are applicable in local regions. We set up a generic cubic box with 1000 cells in each redshift range. The redshift of the box is set to be the central redshift of the given range. Matsubara & Szalay (2002) showed that the precise value of this mean redshift is not a decisive factor when evaluating the Fisher matrix. Instead, the finiteness of the spatial volume and the number density of the objects, i.e., cosmic variance and shot noise, are the main sources of the statistical uncertainty.

Following Matsubara & Szalay (2001), we adopt a coordinate system in which the radial distance s is measured by $s = cz/H_0 = (2997.9h^{-1}\ \mathrm{Mpc})z$, which is an observable quantity, instead of the comoving distance. The latter is a cosmology-dependent quantity requiring to be measured. Consequently, a new notation $h^{-1}\ \mathrm{Mpc}_z$ should be adopted for s instead of h^{-1} Mpc. For the box size, it should be large enough so that it contains a large number of cells with their radii larger than the typical nonlinear scale, and at the same time small enough so that cosmic variance does not severely contaminate the final results. Thus we set the box size $L = 200h^{-1}\ \mathrm{Mpc}_z$ for both the main sample and the LRG sample. Obviously the box size is smaller than the survey volume of each redshift range, therefore, the Fisher matrix should be rescaled according to the ratio of the volume of the box to the total volume.

The fiducial values of the model parameters are set to be $(\Omega_m\ , \Omega_\Lambda\ , \omega_0\ , \omega_a,\ f_B,\ h,\ \sigma_8, n_s) =$ (0.3, 0.7, –1, 0, 0.15, 0.7, 1,1). The bias parameters are expected to vary with samples in different redshift ranges. We take fiducial values $b = 1$ and 2 for the main sample and the LRG sample, respectively. In evaluating the correlation function through the matter power spectrum, we use a set of fitting formulae given by Eisenstein & Hu(1998), which accounts for the effect of baryonic oscillations.

In Figure 1, we plot the expected error bounds of ω_0 and ω_a from the Fisher matrix evaluation of the five different redshift ranges. Here the two parameters ω_0 and ω_a are evaluated simultaneously with all the other parameters held fixed. The survey area is taken to be $1.5\pi\ Sr$ for all the redshift ranges, so that the normalization of Fisher matrix increases with redshift.

From Figure 1, we see a strong correlation between ω_0 and ω_a. This degeneracy is intrinsic, as we will demonstrate later in this paper. It is further noted that the direction of the degeneracy rotates counter-clockwise with the increase of redshift. At the same time, the concentration of the ellipse becomes tighter as the sample redshift increases, partly due to the normalization. As a result, it is expected to be helpful to combine the constraints from different redshift ranges in breaking the parameter degeneracy and imposing further constraint on parameters of dark energy.

In reality, with the same available observing time, a deeper survey usually probes relatively smaller area than a shallow survey. In Figure 2, we plot the expected error bounds of ω_0 and ω_a from the three relatively higher redshift ranges of the previous five, assuming a fixed survey volume for different bins with the value taken to be the volume of the bin with $z:0.25$–0.35. The constraint from the combination of the three redshift ranges is also plotted in the $\omega_0 - \omega_a$ plane. Although the improvement of the concentration level with redshift is no more obvious as in the first case, we can still see clearly the rotation of the degeneracy direction with the redshift. Moreover, it proves to be a promising method combining observations of different redshift ranges to further constrain the parameters.

The strong degeneracy shown in Figures 1 and 2 reflects the way the correlation function intrinsically depends on the dark energy. There are two main physical factors involved, namely, the linear growth factor of density fluctuations and the AP factor. In Figure 3 we plot the degeneracy of ω_0 and ω_a resulting from the two factors separately. The redshift bins are centered at $z_m = 0.3, 0.4, 0.5, 0.8$ and 1.5, respectively, and the bin width is uniformly taken as 0.1. The contour plots are generated following the procedure of Linder (2003b) with 40 data points in each redshift bin. The relative error of each data point is taken to be 0.01. We see that the direction of the degeneracy from the linear growth factor is steeper in the ω_0-ω_a plane than that of the AP factor, and the AP factor is more sensitive to ω_0 as shown by the extension of the ellipse in the ω_0 direction. It is further noted that in both cases the direction of the degeneracy rotates counter-clockwise with redshift, the same as shown in Figures 1 and 2. To make a more direct comparison, we show in Figure 4 the constraining contours from the correlation function analysis for the same redshift bins as in Figure 3. It is seen that the results lie in between the two cases of Figure 3 with the contour direction closer to that of the linear growth factor.

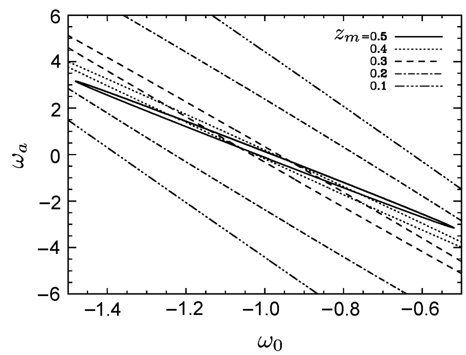

Fig. 1 Expected error bounds of dark energy parameters ω_0 and ω_a, the 1σ uncertainty level of two-parameter joint probability distribution resulting from five redshift ranges.

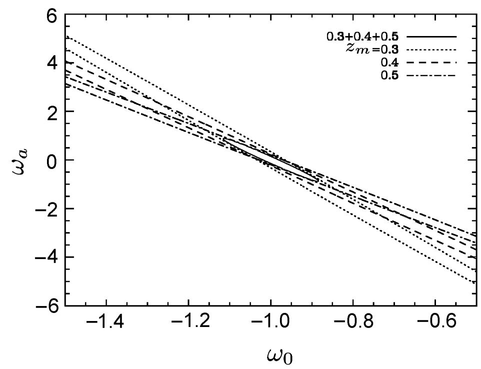

Fig. 2 Expected error bounds of dark energy parameters ω_0 and ω_a, the 1σ uncertainty level of two-parameter joint probability distribution resulting from three relatively higher redshift ranges. The solid line represents the result of the combination with the three redshift ranges.

One should note that in the distant-observer approximation, the separation of two arbitrary cells and the angle between them from the observer are fixed under the fiducial cosmological model. Thus the influence of AP effect is weakened to a great extent. As a result, it is the linear growth factor that plays dominant roles in constraining the equation of state of dark energy.

Comparing Figure 4 with Figure 1, we find that, if the survey depth can be effectively enhanced to $z \sim 1.5$ by adopting some appropriate galaxy sample as tracers, the equation of state of dark energy can be constrained surprisingly well even merely by means of galaxy redshift surveys.

3.2 The General Case

In this case, we restrict our consideration within the LRG sample due to the large budget in calculating the huge complex correlation matrix without the distant-observer approximation.

We consider a realistic redshift range of LRG sample in LAMOST survey $z \sim 0.2 - 0.4$, which is comparable to the SDSS LRG sample distribution that Matsubara & Szalay (2003) took into account. As before, we still set a sub-region of approximately 300 square degree area in the redshift range. Following Matsubara & Szalay (2003), we fill this sub-region with spherical cells of radius $15h^{-1}$ Mpc, assuming nonlinear evolutionary effects are erased by this choice of smoothing radius. We use a cubic closed-packed structure which has the maximum filling factor of 0.74 that can be

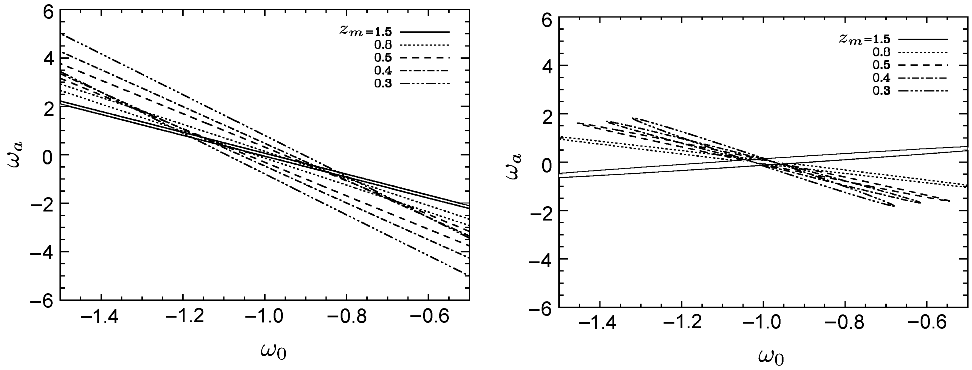

Fig. 3 Idealized results of estimating ω_0 and ω_a. This is purely to illustrate the rotation of degeneracy direction. Left: the result given by the growth factor $D(z)$. Right: the result given by the AP effect factor $H(z)d_A(z)$.

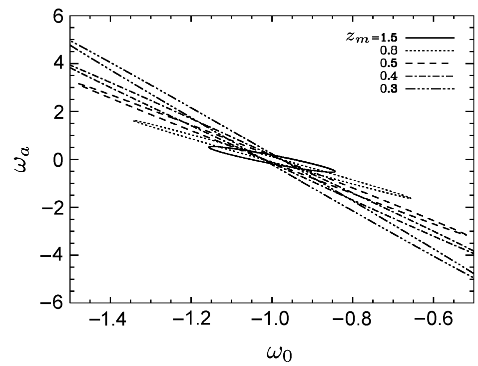

Fig. 4 An idealized case: 1σ uncertainty level of joint probability distribution for ω_0 and ω_a derived from five high redshift ranges. The normalization of Fisher matrix is fixed to be the value of $z_m = 0.5$ redshift range.

filled with spherical cells without overlapping. In total, we place about 1800 cells in the sub-region. The Fisher matrix should still be rescaled according to the ratio of the volume of the sub-region to the total volume.

In Figure 5, we plot the expected error bounds of the two parameters of dark energy ω_0 and ω_a with all the other cosmological parameters fixed at the fiducial values. To compare with the results of the distant-observer approximation, we show in Figure 6 the joint 1σ contour of $z_m = 0.3(0.25 - 0.35)$ bin and $z_m = 0.4(0.35 - 0.45)$ bin under the distant-observer approximation (solid line), along with the results without the approximation in the redshift range of $0.2 - 0.4$ (dotted line). We have adjusted our normalization so that both have the same total volume. It is seen that AP effect, fully taken into account in the case without the distant-observer approximation, helps to reduce the contour significantly.

Also shown in Figure 6 is the joint constraint from bins of $z_m = 0.3, 0.4$ and 0.5 under the distant-observer approximation. The improvement by adding the bin with $z_m = 0.5$ is clearly seen, which demonstrates the potential that LAMOST can contribute to the dark energy research in comparison with that of SDSS. Specifically, the 1σ constraint from two bins of 0.3 and 0.4 is about ω_0: $(-1.2, -0.8)$, ω_a: $(-1.5, 1.5)$. With an additional bin of $z_m = 0.5$, the corresponding constraint becomes ω_0: $(-1.1, -0.9)$, ω_a: $(-0.7, 0.7)$, with improvement by a factor of two. It is expected that the contour will be further reduced if the full AP effect is taken into account by removing the distant-observer approximation.

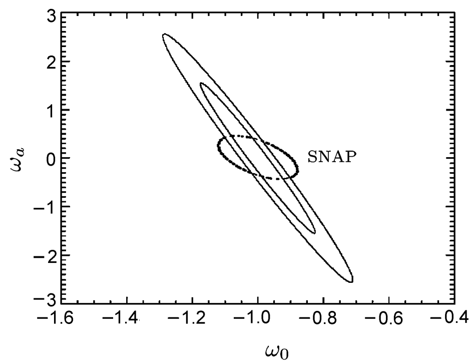

Fig. 5 Expected error bounds of dark energy parameters ω_0 and ω_a derived from the LRG sample in redshift range 0.2–0.4. Inner and outer solid lines represent the 1σ and 2σ uncertainty levels of two-parameter joint probability distribution, respectively. The dashed line shows the 1σ expectation for SNAP with a marginalization over Ω_m (Linder 2003b).

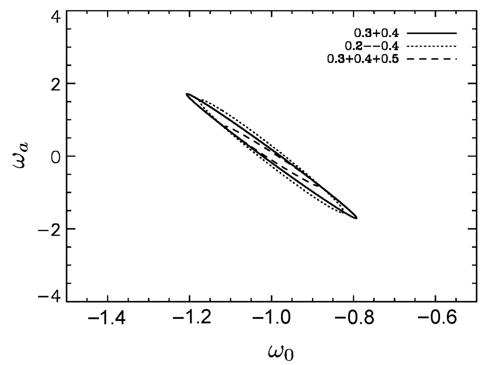

Fig. 6 Expected 1σ error bounds of dark energy parameters ω_0 and ω_a. The solid line is the joint bound from two bins of $z_m = 0.3$ and $z_m = 0.4$ with the distant-observer approximation, the dotted line is the result with $z = 0.2 - 0.4$ without the distant-observer approximation, and the dashed line is the joint bound from three bins of $z_m = 0.3, 0.4$ and 0.5 with the distant-observer approximation.

In Figure 5, we also compare our results with the expected constraints for SNAP given by Linder (2003b). It is shown that there exists a relatively obvious rotation of degeneracy directions between the results of two future observations. SNAP observations are relatively more sensitive to ω_a, whereas the correlation function analysis can constrain ω_0 better. Our previous analyses have indicated that the AP factor, which is imprinted on the correlation function in redshift space, is relatively more sensitive to the evolution of the equation of state in comparison with distance measurement methods. However, one should note that the redshift range we consider here, i.e., $0.2 - 0.4$, is much lower and narrower than that of SNAP, which extends up to $z \sim 1.7$. When more ranges of high redshift are combined, as seen in Figure 4, the constraints on ω_a with correlation function analysis are much better. In any case, the combination of the two results shown in Figure 5 clearly reduces the error bound to a large degree.

4 CONCLUSIONS

We evaluate the Fisher matrices of the galaxy correlation function in redshift space in several different cases, and present the expected error bounds of dark energy parameters. Two dark energy-dependent effects are presented in the analysis. One is the linear growth factor of density perturbations, and the other is the AP factor. Both effects depend on ω_0 and ω_a in a degenerate way, which results in the constraint on ω_0 and ω_a from the analysis of the correlation function exhibiting strong degeneracies. The direction of the degeneracy, however, changes with redshift. Therefore, a promising way to put relatively tight constraints on the equation of state of dark energy is by combining galaxy surveys of different redshift ranges together. In this respect, LAMOST has the potential of making a major contribution to the dark energy studies. For LRG samples, if the volume-limited range can extend to $z = 0.5$, the constraints on ω_0 and ω_a can be improved by a factor of two in comparison with that of $z = 0.4$ achieved by SDSS.

It is a hopeful way as well to combine multiple cosmological observations to constrain the dark energy parameters. The comparison between our result and the result of SNAP (Linder 2003b) shows that, with only statistical errors considered, the method applied in this paper is complementary to the SNIa distance method. While the SNAP observations are more sensitive to ω_a, the correlation analysis can put tighter constraints on ω_0.

It is important to bear in mind the caveats in our analysis, however. First, we set strong priors in the study of the constraints on ω_0 and ω_a, which can result in an under estimation of the error bounds. Secondly, our analysis only takes into account statistical errors without considering systematic ones. The latter, however, may introduce severe limitations on the abilities of a probe. Our future studies will investigate in detail both the effects of different priors and systematic errors.

Acknowledgements We thank T. Mutsubara, E. Linder and B. Feng for helpful discussions, and C. Tao for comments and corrections on the draft. We acknowledge the support from the Computer Center of Peking University. This research was supported in part by the National Natural Science Foundation of China under Grants 10243006 and 10373001, by the Ministry of Science and Technology of China under Grant TG1999075401, and by the Key Grant Project of Chinese Ministry of Education (No. 305001).

References

Alcock C., Paczyński B., 1979, Nature, 281, 358
Allen S. W., Schmidt R. W., Fabian A. C., Ebeling H., 2003, MNRAS, 342, 287
Allen S. W., Schmidt R. W., Ebeling H. et al., 2004, MNRAS, 353, 457
Bahcall N. A., Ostriker J. P., Perlmutter S., Steinhardt P. J., 1999, Science, 284, 1481
Caldwell R. R., 2002, Phys. Lett. B, 545, 23
Caldwell R. R., Doran M., 2005, astro-ph/0501104
Caldwell R. R., Dave R., Steinhardt P. J., 1998, Phys. Rev. Lett., 80, 1582
Eisenstein D. J., Zehavi I., Hogg D. W. et al., 2005, astro-ph/0501171
Eisenstein D. J., Annis J., Gunn J. E. et al., 2001, AJ, 122, 2267
Eisenstein D. J., Hu W., 1998, ApJ, 496, 605
Fan Z. H., Wu Y. L., 2003, ApJ, 598, 713
Feng L. L., Chu Y. Q., Yang X. H., 2000, Chin. Astron. Astrophys., 24, 413
Fosalba P., Gaztanaga E., 2004, MNRAS, 350, L37
Freedman W. L., Madore B. F., Gibson B. K. et al., 2001, ApJ, 553, 47
Garnavich P. M., Jha S., Challis P. et al., 1998, ApJ, 509, 74
Haiman Z., Mohr J., Holder G., 2001, ApJ, 553, 545
Hu W., 2005, Phys. Rev. D, 71, 047301
Huterer D., Cooray A., 2005, Phys. Rev. D, 71, 023506
Jarvis M., Jain B., Bernstein G. et al., 2005, astro-ph/0502243
Knop R. A., Aldering G., Amanullah R. et al., 2003, ApJ, 598, 102
Linder E. V., 2003a, Phys. Rev. Lett., 90, 091301
Linder E. V., 2003b, Phys. Rev. D, 68, 083503
Li M. Z., Feng B., Zhang X. M., 2005, hep-ph/0503268
Matsubara T., 2004, ApJ, 615, 573
Matsubara T., Suto Y., 1996, ApJ, 470, L1
Matsubara T., Szalay A. S., 2001, ApJ, 556, L67
Matsubara T., Szalay A. S., 2002, ApJ, 574, 1
Matsubara T., Szalay A. S., 2003, Phys. Rev. Lett., 90, 021302
Matsubara T., Szalay A. S., Pope A. C., 2004, ApJ, 606, 1
Padmanabhan N., et al., 2004, astro-ph/0410360
Peebles P. J. E., 1980, The Large-Scale Structure of the Universe, Princeton: Princeton University Press
Perlmutter S., Aldering G., Goldhaber G. et al., 1999, ApJ, 517, 565
Rapetti D., Allen S. W., Weller J., 2005, MNRAS, 360,555
Ratra B., Peebles P. J. E., 1988, Phys. Rev. D, 37, 3406
Reese E., 2004, Measuring and Modeling the Universe, from the Carnegie Observatories Centennial Symposia, Edited by W. L. Freedman, 2004, p.138 (astro-ph/0306073)
Riess A. J., Filippenko A. V., Challis P. et al., 1998, AJ, 116, 1009
Riess A. J., Strolger L. -G., Tonry J. et al., 2004, ApJ, 607, 665
Seljak U., Makarov A., McDonald P. et al., 2005, Phys. Rev. D, 71, 103515
Spergel D. N., Verde L., Peiris H. V. et al., 2003, ApJS, 148, 175
Tegmark M., Blanton M., Strauss M. et al., 2004, ApJ, 606, 702
Tegmark M., Taylor A. N., Heavens A. F., 1997, ApJ, 480, 22
Vogeley M. S., Szalay A. S., 1996, ApJ, 465, 34
York D. G., et al. (The SDSS Collaboration), 2000, AJ, 120, 1579